

## Small-displacement monochromator for microdiffraction experiments

Gene E. Ice<sup>a)</sup> and Jin-Seok Chung  
*Oak Ridge National Laboratory, Oak Ridge, Tennessee 37830*

Walter Lowe, Ernest Williams, and Joel Edelman  
*Howard University, Washington, DC 20059*

(Received 24 November 1999; accepted for publication 4 January 2000)

We describe the design, construction, and performance of the MHATT-CAT microdiffraction x-ray monochromator. This monochromator is specially engineered for x-ray microdiffraction experiments with a high brilliance undulator source. The monochromator passes a small emittance beam, suitable for focusing to submicron size with submilliradian divergence. Over its energy range of 8–22 keV the absolute energy calibration is better than 2 eV and scans of  $\pm 1$  keV show no measurable hysteresis. The monochromator operates with a simple water-cooled first crystal and shows no measurable warm-up time. Horizontal linear bearings allow the monochromator crystals to be rapidly inserted or removed from the beam. Slits before and after the monochromator work to pass broad bandpass or monochromatic x-ray beams at the same vertical height. The monochromatic beam direction is adjusted so the monochromatic and broad bandpass beams are coaxial. The design and performance of the monochromator allows efficient collection of microdiffraction data when coupled to a nondispersive Kirkpatrick–Baez focusing mirror pair. © 2000 American Institute of Physics. [S0034-6748(00)01805-0]

### I. INTRODUCTION

The recent availability of ultrabright third-generation synchrotron sources has created an opportunity to map the crystallographic phase, texture, and strain of materials with micron or submicron spatial resolution.<sup>1</sup> With single crystal specimens it may sometimes be possible to utilize crystallographic techniques similar to those used with large x-ray beams. For fine-grained polycrystalline samples however, new methods are required; when a fine-grained polycrystalline sample is rotated, not only the incident angle, but also the very grains illuminated by the x-ray beam change (Fig. 1). In addition, the sphere-of-confusion for even state-of-the-art goniometers causes the sample position to move relative to the incident beam as the sample is rotated.<sup>2</sup> As a result, diffraction methods that avoid rotation of the sample are desirable for x-ray microdiffraction on fine-grained polycrystalline samples.

Laue diffraction offers a method of determining the orientation of a single crystal without sample rotations. Laue diffraction can be extended to the measurement of strain, with high-precision angular measurements of the Laue pattern and with high precision measurements of the energy of one or more reflections.<sup>1</sup>

Various techniques have been used to measure the x-ray energies of microdiffraction Laue spots.<sup>3</sup> Rebonato *et al.*,<sup>4</sup> Cargille *et al.*,<sup>5</sup> and Yamamoto *et al.*<sup>6</sup> have demonstrated strain mapping with solid-state detectors. Evans-Lutterod<sup>7</sup> has demonstrated measurements with a diffracted beam monochromator that can be rotated about the sample.

Compared with alternative techniques, an incident beam monochromator has both major technical advantages and

major technical challenges. The chief advantage of an incident beam monochromator is the intrinsically good energy resolution which is at least two orders of magnitude better than for state-of-the-art solid-state detectors. Indeed x-ray monochromators with milli-electron volt energy resolution can be designed for specialized applications.<sup>8</sup> For precision absolute strain measurements, a monochromator with  $\sim 4$  eV energy resolution *and even better absolute accuracy* at 20 keV is desirable.

Incident beam x-ray monochromators on third generation synchrotron sources are challenged by the need for thermal and mechanical stability under a high thermal-flux x-ray beam.<sup>9</sup> With x-ray microdiffraction it is also important to maintain a constant offset as the beam is tuned or cycled between white and monochromatic modes; fixed offset is necessary to preserve the focal position on the sample. For example, with focusing optics of magnification  $M$ , a beam displacement  $\delta$  results in a motion at the focus of  $\delta M$ . With a vertical magnification of  $\sim 1/300$ , vertical displacements of less than  $30\text{ }\mu\text{m}$  will move the focal spot less than  $0.1\text{ }\mu\text{m}$ . Angular stability is even more important. Angular stability of  $\sim 1\text{ }\mu\text{rad}$  is required to hold the focal position to better than  $0.1\text{ }\mu\text{m}$ .

Fortunately, the very nature of microdiffraction experiments simplifies the thermal load and beam stability problems of a microdiffraction monochromator. Typically only about 0.1% of the thermal load from a high brilliance third generation undulator is within the useable emittance for microdiffraction. As described in Ref. 9, this brings the total power on the first crystal of a monochromator into the range which can be handled by water-cooled optics. A detailed theoretical discussion of the anticipated thermal distortions on a water-cooled microbeam monochromator crystal is

<sup>a)</sup>Electronic mail: icege@oml.gov

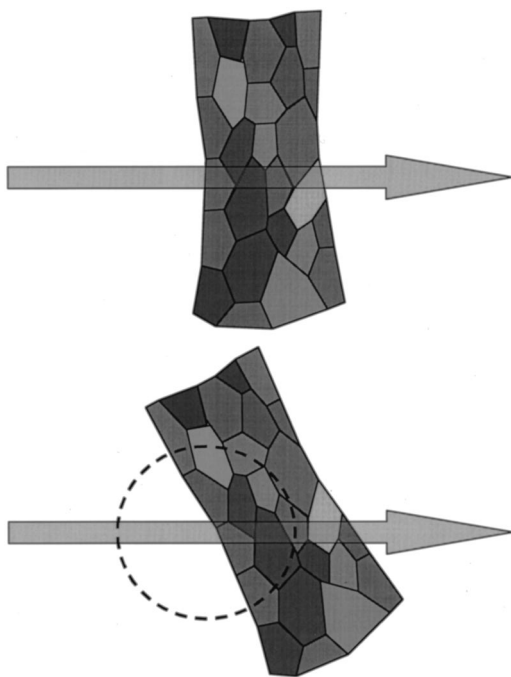


FIG. 1. In a polycrystalline sample, the grains illuminated by a penetrating x-ray beam change even if the sample is rotated with negligible translations. With a real goniometer, however, there is a finite sphere of confusion which introduces additional beam motion relative to the sample grains.

given in Ref. 9. In general the distortions do not substantially decrease the source brilliance under most conditions.

## II. SMALL DISPLACEMENT MONOCHROMATOR PERFORMANCE GOALS

### A. Beam offset

Because the x-ray beams required for x-ray microprobe experiments are small, it is possible to consider the development of an ultrasmall displacement monochromator. This has major advantages for x-ray microprobe experiments since it allows the focusing optics to remain fixed while the focused beam is cycled between white and monochromatic conditions or scanned in energy.

The MHATT-CAT micromonochromator is designed to pass both “white” beams, and monochromatic beams through the same exit slit. The monochromatic beam offset is  $\sim 1$  mm. To reduce the thermal load on the second slit, the first slit restricts the white beam both in the white and mono modes. For a nondispersive monochromator, the beam offset  $O$  is almost exactly twice the gap,  $G$  between the crystal faces for angles less than  $20^\circ$ :

$$O = 2G \cos \theta. \quad (1)$$

Note the highest angle of operation for the micromonochromator is  $\sim 14^\circ$  with  $\text{Si}_{111}$ . At this angle, a gap of  $500 \mu\text{m}$  will result in a beam displacement of  $970 \mu\text{m}$ . At the lowest angle of operation ( $5^\circ$ ) the beam displacement for the same  $500 \mu\text{m}$  gap is  $996 \mu\text{m}$ . The required gap is therefore  $\sim 500 \mu\text{m}$ .

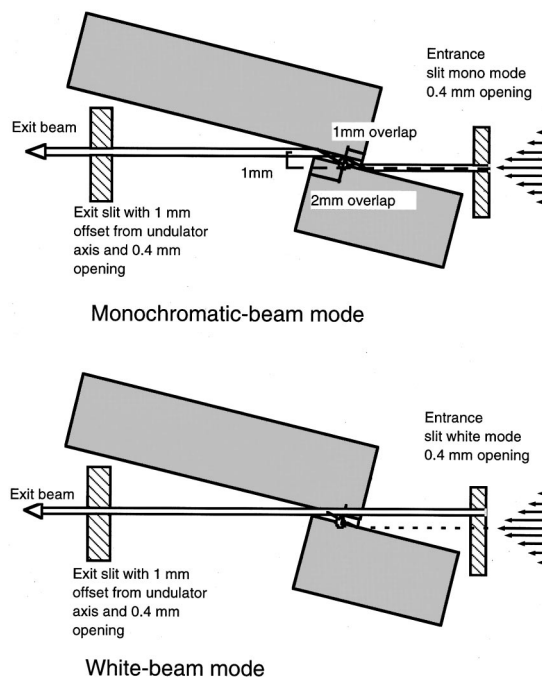


FIG. 2. Slit and crystal geometry for the MHATT-CAT small displacement monochromator. In the monochromatic mode (top) the water-cooled first slit passes an  $\sim 400 \mu\text{m}$  high beam onto the first water-cooled  $\text{Si}_{111}$  crystal. The beam is reflected upward and then directed onto the second slit by the matched  $\text{Si}_{111}$  crystal. The second slit defines the vertical height at which the beam emerges from the monochromator. In the white-beam mode the crystals are translated horizontally until they no longer intercept the x-ray beam. The first slit also translates with the crystals and has a 1 mm step which centers its aperture on the aperture of the second slit. Hence, the beam vertical position is again defined by the second slit.

### B. Beam parallelism

Although the design illustrated in Fig. 2 ensures that the beam exits from the same vertical aperture with or without the monochromator, there is a small angular difference between the monochromatic and white beams that exit from the final aperture. The 1 mm displacement at 30 m corresponds to an angular change of  $30 \mu\text{rad}$ . With 200:1 vertical demagnification this will result in a displacement of the beam by  $\sim 3 \mu\text{m}$ . This vertical offset can be corrected by sample translation or by tilting the x-ray mirror  $15 \mu\text{rad}$ . Tilting, however, results in a small ( $\sim 0.5\%$ ) change in the focal length with about a 30% blurring of the x-ray beam spot.

A more elegant solution is to correct the  $\sim 30 \mu\text{rad}$  difference between the white and monochromatic beams by heating the second crystal. The temperature difference  $\Delta T$  required to tilt a Si (111) reflected beam  $0.03 \text{ mrad}$  depends on the x-ray energy;  $\Delta T(^{\circ}\text{C}) \sim 2.9E \text{ (keV)}$ .

### C. Beam bandpass/brilliance

The bandpass onto the sample and the solid angle subtended by the detector determine the number of diffraction spots detected with Laue diffraction. For a simple face-centered-cubic (fcc) metal lattice, the reciprocal space volume per reflection is about  $(1/2)(1/3.5^3) = 0.012 \text{ \AA}^{-3}$ . In a geometry where an area detector at  $90^\circ$  to the beam is used to collect the diffraction spots, the volume of reciprocal space collected is given by  $(d\lambda/\lambda)(1/\lambda^3)(A/R^2)$  as shown in

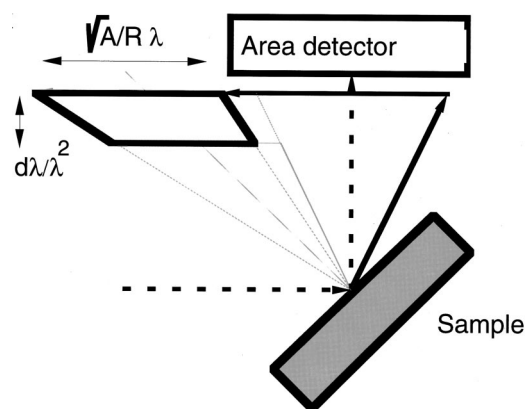


FIG. 3. Reciprocal space volume measured is determined by the solid angle of the area detector and the energy bandpass.

Fig. 3. Here  $A/R^2$  is the solid angle subtended by the detector,  $\lambda$  is the x-ray wavelength, and  $d\lambda/\lambda$  is the bandpass of the x-ray beam. The number of reflections which can be collected for a typical fcc metal is therefore given by

$$N \approx 85 \frac{d\lambda}{\lambda} \frac{1}{\lambda^3} \frac{A}{R^2}. \quad (2)$$

In typical experiments, a solid angle of about 0.25–1 ST can be collected;  $A/R^2 < 1$ . Therefore, at 20 keV at most ten reflections will be collected with a 3% bandpass. We note that at 10 keV a 20% bandpass will collect at most eight reflections and from 6–10 keV about ten reflections can be intercepted.

Bandpass and x-ray energy can therefore be adjusted to optimize the experimental conditions. Too few reflections and it is difficult to index the pattern. Too many reflections and it is difficult to index overlapping patterns from multiple grains. High energy reflections (high indices) have narrower Darwin widths. Low energy reflections have greater integrated reflectivity. In addition, angular accuracy is improved with greater distance to the detector for a given pixel size (decreased solid angle subtended).

The bandpass of an undulator can be controlled by tapering the undulator or by collecting off-axis radiation. For cases where the highest brilliance monochromatic radiation is needed part of the time, it is convenient to tailor the beam bandpass by collecting on or off axis. Directly on axis, undulator radiation from a type A undulator at the Advanced Photon Source (APS) has a narrow  $\sim 1\%$  bandpass. Off axis the spectrum is redshifted and broadened. This broadened bandpass greatly simplifies experiments such as Laue diffraction. This ability to control the incident beam spectrum has been used in the design of the microbeam monochromator to tailor the spectrum for highest brilliance when in monochromatic mode and for increased bandpass when used in “white-beam” mode for Laue diffraction. The spectra from a type A undulator on axis and vertically off axis by 1 mm is shown in Fig. 4. The design goals of the MHATT-Cat microbeam monochromator are summarized in Table I.

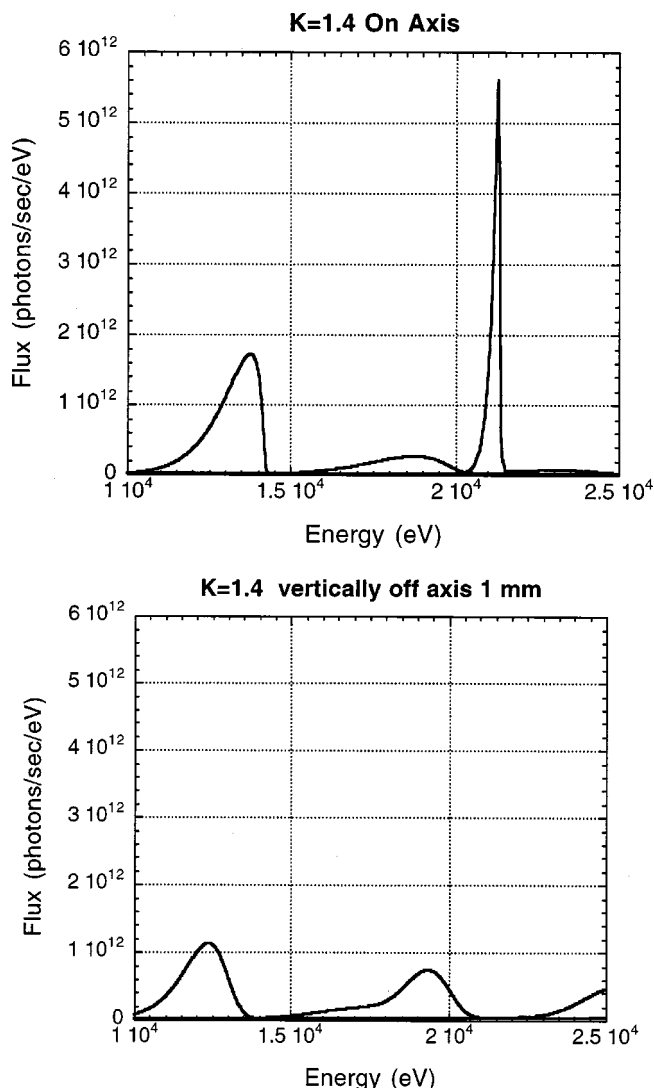


FIG. 4. Undulator A spectrum through a 0.1 mm wide by 0.3 mm high aperture at 30 m from the source with  $K=1.4$ . The spectrum is shown on axis and vertically off axis by 1 mm.

### III. MECHANICAL DESIGN

To achieve the design goals outlined above, a rugged and mechanically stable design was adopted. The key elements of the design are a thermally stable incident beam vertical slit, a rigid, two-crystal small-displacement monochromator, and a high-precision beam defining the vertical exit slit (Fig. 5).

#### A. Entrance and exit slits

The entrance and exit slits are fabricated from precision machined Cu blades mounted on a rigid frame which rotates through a flex pivot™ support.<sup>10</sup> The angle of the blades is controlled by a nanomover™ stepping motor driven linear actuator produced by Mellos Griot.<sup>11</sup> The flex pivot axis is at  $15^\circ$  with respect to the beam axis so the x-ray beam is spread along the vertical slit to reduce local heating. Experience has shown that this design is very stable, although in future designs, the blades will include both Cu masks for thermal reasons and W blades to reduce the harmonic radiation which passes through the monochromator system.

TABLE I. Design goals for the MHATT-Cat microdiffraction monochromator.

Desirable microbeam monochromator property	Goal	Measured
Bandpass for monochromatic	0.02%	0.02%
Bandpass for “white beam conditions”	>5%	>5%
Energy range	8–22 keV	8–22 keV
Energy accuracy	<2 eV at 20 keV	<2 eV from 8–21 20 keV
Mono/white beam displacement	negligible	<0.5 $\mu\text{m}$ 14–22 keV
Mono/white beam parallelism	negligible	negligible (<5 $\mu\text{rad}$ )
Hysteresis during energy scans and when cycling between white and monochromatic conditions	negligible	negligible (<0.1 eV)
Switching time between mono and white beams	<1 s	<3 s

Both front and rear slits can be water cooled, although to date it has not been necessary to cool the second slit pair. The first slit includes a 1 mm step which corresponds to the 1 mm offset of the beam when cycling between polychromatic and monochromatic operations. A schematic of the beam conditions relative to the monochromator and slits for various conditions is shown in Fig. 2.

### B. Crystal monochromator assembly

The two-crystal x-ray monochromator also is based on flex pivot<sup>TM</sup> rotations. A rectangular cage is used to hold the first and second crystal subassemblies. These assemblies are designed to allow for a  $\chi$  (roll) tilt of the first crystal and for a  $d\theta$  (pitch) tilt of the second crystal. The overall cage assembly is also driven by a nanomover<sup>TM</sup> actuator which is coupled to the crystal cage through a linear ball bearing stage and two flex pivots.

The monochromator components are housed in an ultra-high vacuum stainless steel chamber. The entire chamber is supported on parallel linear bearings with a stepping motor driven lead screw to laterally translate the monochromator crystals into or out of the incident beam. Vacuum forces acting on the actuators through bellows feedthroughs are

counteracted by simple springs. A picture of the assembled microbeam monochromator with the main access flange removed is shown in Fig. 6.

## IV. MONOCHROMATOR PERFORMANCE

### A. Absolute energy calibration

The monochromator absolute energy scale and resolution was calibrated by measuring the near edge structure of standard metal foil samples. The energy passed by the monochromator depends on the angle of the crystals with respect to the incident beam. The crystal angle is driven through a sine bar mechanism with a theoretical energy/motor step response given by

$$E(\text{keV}) = 1.976R/(x + x_0). \quad (3)$$

Here  $x$  is the position of the precision translator,  $x_0$  is an offset, and  $R$  is the length of the sine bar lever arm. The offset  $x_0$  was determined from the measured position of the Mo edge.

Near edge absorption edges of Cu, Mo, Sr, and Rh were measured and compared to the literature edge values. The *absolute calibration* of the monochromator was found to be better than  $\pm 0.5$  eV over the 8–22 keV nominal range of the monochromator.

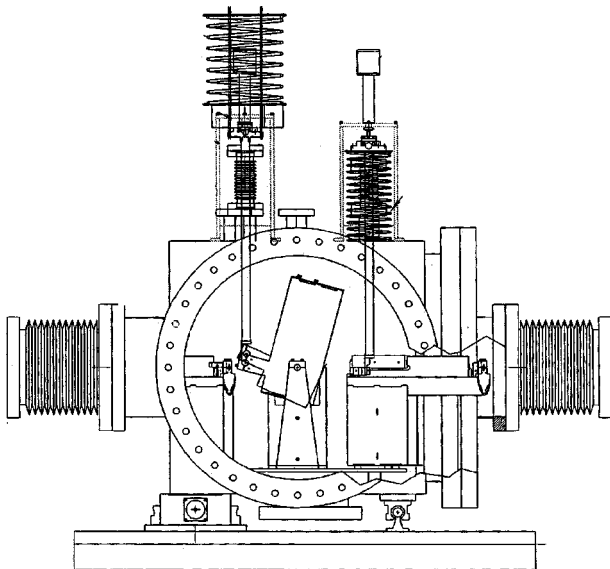


FIG. 5. Micromonochromator box showing the actuator for the monochromator crystal cage and the actuator for the entrance slit. The entire box assembly is on linear bearings so it can be moved into and out of the beam.

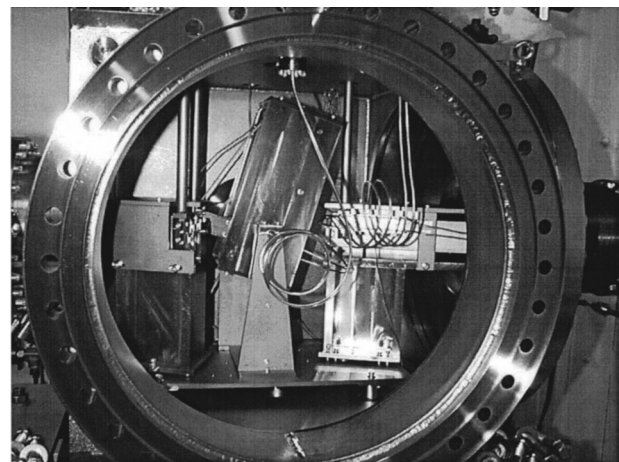


FIG. 6. View of the MHATT-CAT microdiffraction monochromator as seen through the main access flange.

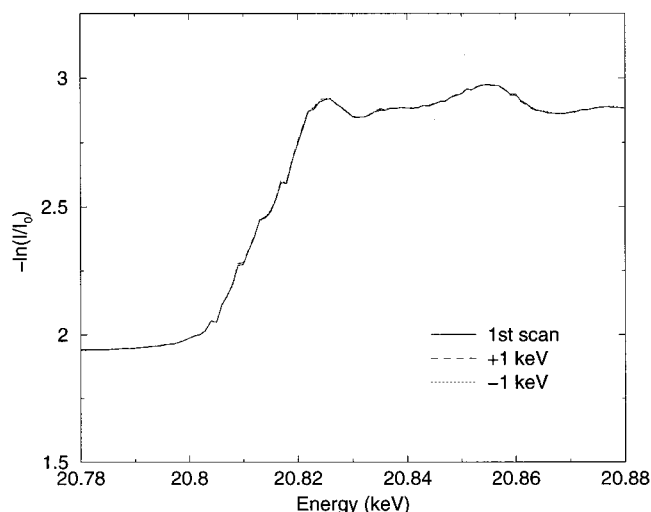


FIG. 7. Three scans of the Mo edge showing no measurable hysteresis after the monochromator was driven  $\pm 1$  keV from the edge.

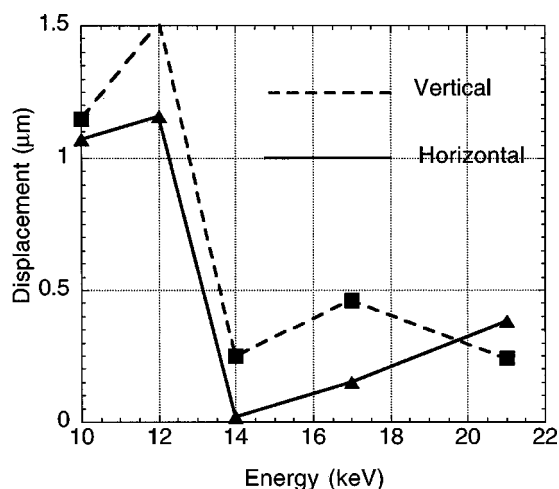


FIG. 8. Displacement of the monochromatic focal spot from the white beam focus as a function of x-ray energy.

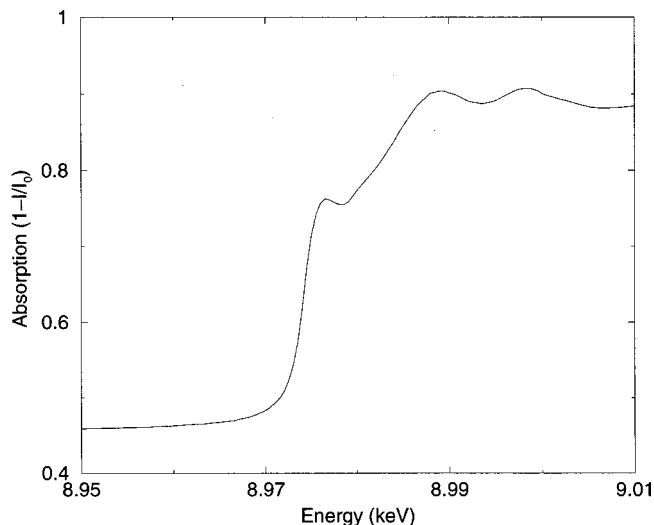


FIG. 9. Cu K edge showing pre-edge feature.

## B. Hysteresis

Monochromator reproducibility and hysteresis were checked both over short ( $\sim \pm 1$  keV) scans and over the entire range of the monochromator. As shown in Fig. 7, scans of less than 1 keV show no visible hysteresis. Scans of  $\sim 10$  keV show  $\sim 0.5$  eV backlash. Note the steps in the Mo edge scan are believed to be the result of roundoff errors in the control software and do not appear below  $\sim 15$  keV.

## C. Warm-up time

Because of the small thermal mass of the monochromator crystals and because of the small power load (of order 1–4 W), there was no observable warm-up time for the instrument after beam turn on or after the monochromator was inserted into the beam. Warm up was checked by measuring the Mo edge immediately after insertion of the monochromator and 1 h after insertion of the monochromator. No observable displacement of the edge position was detected.

## D. Beam displacement

The beam displacement was checked by measuring the position of a standard gold wire with monochromatic and with polychromatic beams. As shown in Fig. 8, both the vertical and horizontal focal spot positions with the two beams are within the focal spot resolution.

## E. Energy resolution

The energy resolution of the monochromator was inferred from the Cu near-edge spectra. The shape of the near-edge feature in Fig. 9 indicates an energy resolution of  $\sim 2$  eV or better at 9 keV. This is near the theoretical Darwin width limited resolution of the  $\text{Si}_{111}$  monochromator crystals.

## V. DISCUSSION

An x-ray monochromator has been fabricated with properties optimized for x-ray microdiffraction experiments at a third generation synchrotron source. The monochromator has demonstrated outstanding mechanical and thermal stability and provides an absolute calibration for the incident x-ray energy on a sample. No measurable hysteresis is observed for scans of  $\pm 1$  keV. The simple, yet rugged, design based on flex pivots and a water-cooled first crystal appears to be a good choice for the microdiffraction experiments envisioned with this instrument.

## ACKNOWLEDGMENTS

Research performed on the MHATT-CAT insertion device beamline at the advanced photon source which is supported by the Department of Energy Office of Basic Energy Science is acknowledged. Two of the authors (G.E.I. and J.S.C.) were supported by the Division of Materials Sciences, U.S. Department of Energy under Contract No. DE-AC05-96OR22464 with Lockheed Martin Energy Systems. The authors, wish to gratefully acknowledge the help of Rheinhardt Pahl, John Tischler, Paul Zchack, and Richard Boyce in the micromonochromator fabrication, assembly, and testing.

- <sup>1</sup>J. S. Chung and G. E. Ice, J. Appl. Phys. **86**, 5249 (1999).
- <sup>2</sup>I. C. Noyan, S. K. Kaldor, P. C. Wang, and J. Jordan-Sweet, Rev. Sci. Instrum. **70**, 1300 (1999).
- <sup>3</sup>G. E. Ice, Nucl. Instrum. Methods Phys. Res. B **24/25**, 397 (1987).
- <sup>4</sup>R. Rebonato, G. E. Ice, A. Habenschuss, and J. C. Bilello, Philos. Mag. A **60**, 571 (1989).
- <sup>5</sup>P. C. Wang, G. S. Cargill III, and I. C. Noyan, Mater. Res. Soc. Symp. Proc. **375**, 247 (1994).
- <sup>6</sup>N. Yamamoto and Y. Hosokawa, Jpn. J. Appl. Phys., Part 2 **27**, L2203 (1988); N. Yamamoto and S. Sakata, *ibid.* **34**, L665 (1995).
- <sup>7</sup>K. Evans-Lutterodt (private communication).
- <sup>8</sup>T. S. Toellner, M. Y. Hu, W. Sturhan, K. Kroft, and E. E. Alp, Appl. Phys. Lett. **71**, 2112 (1997).
- <sup>9</sup>G. E. Ice, B. Riemer, and A. Khounsary, Proc. SPIE **2856**, 226 (1996).
- <sup>10</sup>Melles-Griot Corp. Nanomover™, <http://www.mellesgriot.com/pdf/463.pdr>.
- <sup>11</sup>Lucas Aerospace Flex-pivot™, <http://Lucasuttica.com>.